Food Chemistry 311 (2020) 126017

Contents lists available at ScienceDirect

Food Chemistry

journal homepage: www.elsevier.com/locate/foodchem

Impact of water degumming and enzymatic degumming on gum mesostructure formation in crude soybean oil

Tatiana Nikolaeva[a,b], Tim Rietkerk[c], Arjen Sein[c], Robert Dalgliesh[d], Wim G. Bouwman[e], Evgenii Velichko[e], Bei Tian[e], Henk Van As[a,b,*], John van Duynhoven[a,b]

[a] Laboratory of Biophysics, Wageningen University, Stippeneng 4, 6708 WE Wageningen, the Netherlands
[b] MAGNEtic Resonance Research FacilitY (MAGNEFY), Stippeneng 4, 6708 WE Wageningen, the Netherlands
[c] DSM Biotechnology Center, Alexander Fleminglaan 1, 2613 AX Delft, the Netherlands
[d] LARMOR Beamline, ISIS Neutron and Muon Source, UK
[e] Faculty of Applied Sciences, Delft University of Technology, Mekelweg 15, 2629 JB Delft, the Netherlands

ARTICLE INFO

Keywords:
Water degumming
Enzymatic degumming
Phospholipid
Lamellar liquid-crystalline structure

ABSTRACT

Phospholipid gum mesostructures formed in crude soybean oil after water degumming (WD) and enzymatic degumming (ED) were studied at a range of phospholipid and water concentrations. For ED, phospholipase C (PLC), phospholipase A2 (PLA2) and a mixture of phospholipases Purifine 3G (3G) were used. Both WD and ED resulted in lamellar liquid-crystalline phases, however, of different topology. The dependence of the bilayer spacings (as observed by SANS and SAXS) on the ratio between amount of water and amphiphilic lipids differed for WD and PLA2 ED vs PLC and 3G ED. This difference was also observed for dynamics at molecular scale as observed by time-domain (TD) NMR and attributed to partial incorporation of diglycerides and free fatty acids into gum bilayers after PLC and 3G ED. Feasibility of using TD-NMR relaxometry for quantification of the gum phase and estimation of degumming efficiency was demonstrated.

1. Introduction

Degumming is a major refining step to remove phospholipids (PLs) as gums from crude oils, in order to obtain high qualitative edible oil products (Dijkstra, n.d.; Sagalowicz et al., 2016). Water degumming (WD) is the traditional refining process effectuated by hydration of PLs and their self-assemby into a lamellar liquid-crystalline mesophase (Lei, Ma, Kodali, Liang, & Ted Davis, 2003; Sein, Hitchman, & Dayton, 2019). The formed WD gums are usually separated from the oil phase by gravitational forces. The separation efficiency of degumming processes is in part defined as amount of the retained neutral oils in the gum. Due to the association of neutral oil with the lamellar mesophases in the gum the separation efficiency of WD is poor (Sein et al., 2019). A well-known alternative to WD is enzymatic degumming (ED), performed by phospholipases that hydrolyze phospholipids and, thus, significantly improve separation efficiency (Dayton & Galhardo, 2014; Sein et al., 2019). So far, most investigations into ED focussed on the chemical characterization of the enzymatic conversion of PLs into their post-reaction products (Cerminati et al., 2019; Dijkstra, 2011; Jiang, Chang, Wang, Jin, & Wang, 2014; Sein et al., 2019; Xie & Dunford, 2017; Ye et al., 2016). In normal industrial-scale WD, the obtained gums are thick (viscous) dispersions of polar lipids, neutral lipids and water. In ED the resulting gum phase is typically much smaller in volume, less viscous but still turbid, because it still contains lipidic components. Microscopic investigations have shown that these lipids still assemble into a lamellar liquid-crystalline phase, yet from a different nature than the lamellar liquid-crystalline phase coming from WD (Sein et al., 2019). More detailed structural investigations on the impact of the different degumming treatments on gum mesostructures are however lacking. Our current insights in the mesoscale structure of gum-like systems are mainly based on binary models consisting of single PLs and water (Kučerka, Pencer, Sachs, Nagle, & Katsaras, 2007; Nagle & Tristram-Nagle, 2000). In these binary model systems, PLs occur as bilayers separated by water layers, comprising a swollen lamellar liquid-crystalline phase, mostly existing as curved mesostructures, such as multi-lamellar vesicles and stacks of bilayers, either planar or curved on the micron scale. In a previous study (Lei et al., 2003) a partial phase diagram was constructed of the soybean oil/PL/water model system, which can be considered as a model for gums formed in oil after WD. Based on investigations of the swelling capacity of PLs at various PL-to-water ratios, it was concluded that under industrially relevant WD conditions, gums exist as hydrated PLs in a lamellar liquid-crystalline

* Corresponding author at: Laboratory of Biophysics, Wageningen University, Stippeneng 4, 6708 WE Wageningen, the Netherlands.
E-mail address: henk.vanas@wur.nl (H. Van As).

https://doi.org/10.1016/j.foodchem.2019.126017
Received 17 July 2019; Received in revised form 28 November 2019; Accepted 3 December 2019
Available online 12 December 2019

(LC) phase (Lei et al., 2003).

To the best of our knowledge no detailed investigation on the impact of ED on gum mesostructures has been performed to date. Due to the different specificities of phospholipases currently in use, resulting PL compositions will vary significantly between different ED treatments. Since formation of LC gum phases is strongly defined by PL composition, their mesostructure should be different between ED treatments. No systematic study as to date has been carried out on the impact of ED on polar lipid composition and resulting gum mesostructure. This lack of detailed insights in modifications of gum mesostructures impedes optimisation of both WD and ED processes and also hampers downstream processing of gums (Dijkstra, 2011; Sen Gupta, 1986; Ye et al., 2016). We hypothesized that upon ED: 1) amphiphilic lysophospholipids become incorporated in the gum bilayers, 2) due to their different shape this will induce curvature of gum bilayers and 3) more neutral enzymatic conversion products will migrate to the oil phase. In order to verify these hypotheses, we characterized gum mesostructures after WD and ED using phospholipase A2 (PLA2), phospholipase C (PLC), or a mixture of phospholipases Purifine 3G (3G), under industrially relevant temperature and water concentrations. The 3G ED process involved a mixture of PLC, phosphatidyl-inositol-specific PLC, PI-PLC, and a minor amount of PLA2, and it is known for its highly efficient conversion of PLs into predominantly diglycerides (DGs), phosphates, some free fatty acids (FFAs) and some lysophospholipids (LPLs) (Sein et al., 2019). An overview of the expected enzymatic conversion products is given in Fig. 1(A). In order to establish relations between amphiphilic lipid composition and mesostructure ^{31}P and ^{1}H quantitative NMR (qNMR) analyses were performed (Rijn, Lankhorst, Groen, Muntendam, & Souza, 2019; Van Duynhoven, van Velzen, & Jacobs, 2013). Polarized light microscopy (PLM) and scanning electron microscopy (SEM) were used to obtain a direct view on gum microstructure. SANS and SAXS were used to estimate thickness of the hydration water layers by quantifying the repeating distance between the bilayers d (spacings). For the SANS experiments, WD and ED was mimicked using D_2O instead of H_2O, in order to enhance contrast and specifically assess the water layers between the PL bilayers (Fig. 1(B)). ^{2}H NMR spectroscopy and ^{1}H time-domain (TD) NMR T_2 relaxometry were used to obtain information about molecular mobility in the gum mesophase and its overall quantification. We hypothesized that T_2 relaxometry would be able to distinguish the molecular mobility of water and hydrated headgroups from the rigid hydrophobic layer consisting of packed alkyl chains (Fig. 1(B)). Furthermore, we investigated whether TD-NMR T_2 relaxometry can be used to quantify the amount of gum in gum/oil dispersions upon the various degumming treatments.

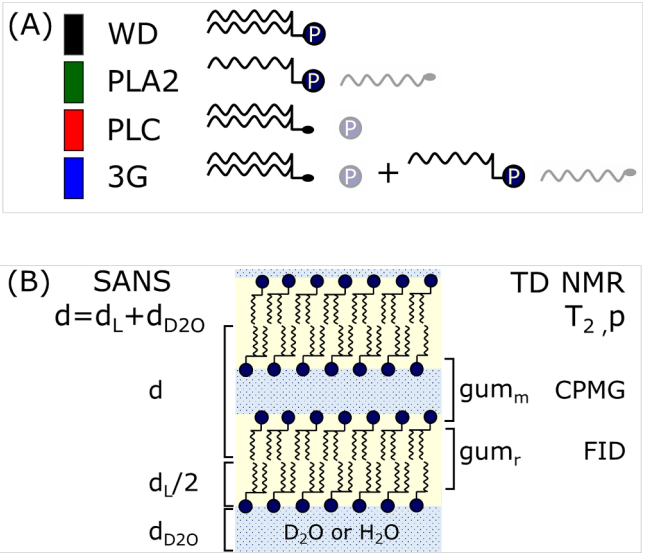

Fig. 1. (A) Schematic representation of the impact of water degumming (WD – black), phospholipase C (PLC – red), phospholipase A2 (PLA2 – green) and their mixture Purifine 3G (3G – blue) enzymatic degumming (ED) on phospholipids (PLs) in oil. (B) A schematic picture of a PL bilayer and its mesostructural characterization by SANS and time-domain (TD) NMR T_2 relaxometry. The spacings (d) obtained from SANS experiments are determined by dimensions of amphiphilic lipids (d_L) and a water layers (d_{D2O}). From FID-CPMG NMR relaxometry T_2 values and proton populations (p) can be obtained for the mobile aqueous layer ($p(gum_m)$, CPMG) and the rigid hydrophobic layer ($p(gum_r)$, FID) consisting of packed alkyl chains. (For interpretation of the references to colour in this figure legend, the reader is referred to the web version of this article.)

2. Materials and methods

2.1. Materials

Crude soybean oil was obtained as Expander Soybean, DSM. The crude soybean oil contained phosphatidylcholine (PC) 0.83w/w%, phosphatidylethanolamine (PE) 0.57w/w%, phosphatidylinositol (PI) 0.51w/w%, phosphatidic acid (PA) 0.23w/w%, free fatty acids (FFAs) 0.21w/w% and diglycerides (DGs) 0.62w/w%. Lecithin was obtained as Leciplus F NMG # 71CMAS2001 by Cereal Docks Food (Italy), which contained 30-40w/w% phospholipids (PLs) with a similar PL profile as crude soybean oil, the remaining part being predominantly triglyceride (TG) oil. The total PL concentration in the crude oil was 2.2w/w%, according to compositional analysis by ^{31}P NMR. PL-enriched oil samples were obtained by adding lecithin in weight concentrations of 12.1 and 27.5w/w% in order to end up with estimated total PL concentrations of respectively 6 and 12w/w%. All reported PL concentrations of the enriched-oil samples were based on actual compositional analyses performed by ^{31}P NMR. Phospholipases were provided by DSM Food Specialties (Delft, the Netherlands): phospholipase A2 (PLA2), phospholipase C (PLC) and Purifine® 3G (3G). The PLA2 enzyme was produced by a selected strain of *Aspergillus niger*. The PLC enzyme was produced by a selected strain of *Pichia Pastoris*, a PI specific phospholipase C enzyme was produced by a selected strain of *Pseudomonas fluorescence*. Purifine® 3G was a combination of three separate phospholipase enzymes [PLC, PI-PLC and PLA2].

2.2. Sample preparation

Samples were prepared in a manner that mimicked industrial WD and ED processes. High-shear mixing (using an Ultra Turrax) during 15 min at full power was applied at ambient temperature to homogenize the crude oil or crude oil with aliquots of lecithin. The homogenized oil was weighed out as 100 or 50 or 10 g aliquots in a 250 mL or 20 mL screw-top Erlenmeyer flask or glass vial, respectively. The samples were placed on a 10-position digital magnetic hotplate stirrer to heat the samples up to 55–60 °C, while mixing at 550RPM. The enzyme solutions were prepared separately by dispersing the phospholipases in H_2O or D_2O. Water was added as either D_2O (99.9 atom%, Cambridge Isotope) or H_2O. Samples prepared with D_2O were used for SANS and ^{2}H NMR experiments. After adding water or the enzyme solutions to crude oil the system was homogenised with the Ultra Turrax during 15 s. Subsequently, the samples were put on the magnetic hotplate stirrer for 5 h in order to achieve near complete conversion. WD was performed at the same conditions by adding D_2O or H_2O at the required concentration. Each type of samples had at least two replicates.

2.3. PLM and SEM

Polarized light microscopy (PLM) images of the oil/gum systems were observed by an Olympus BX53 light microscope (Olympus Nederland B.V., Zoeterwoude, the Netherlands), using bright field and crossed polar mode at room temperature. Images were recorded by a digital camera. To obtain electron microscopy images the oil/gum

samples were rapidly frozen in slushed nitrogen and cryo-fractured by a razor blade knife using a QuorumTech PP3000T cryo-prep unit under high vacuum conditions (10–6 mBar) and a temperature of −135 °C. Freshly made fractured surfaces were coated with a conductive Ir layer for 60 s at 20 mA using the in-line coater. Samples were transferred into a Versa 3D HR FEG-Scanning Electron Microscope (Thermofisher Scientific, formerly FEI) equipped with a cryo-stage while maintaining the cryo conditions. The samples were observed at a beam voltage of 5 kV and the images were recorded using an Everhart Thornley Secondary Electron Detector.

2.4. Lipid compositional analysis by ^{31}P quantitative NMR

The detailed description of the NMR quantification of lipid compositions has been provided elsewhere (Rijn et al., 2019). In short, homogenised oil/gum samples (native crude oil ~300 mg, crude oil enriched with lecithin 12.1w/w% ~150 mg and 27.5w/w% ~75 mg) were mixed with 1 mL of deoxycholic acid (DOC) buffer. The DOC buffer was prepared by dissolving 25 g of DOC (97 + %, Sigma-Aldrich), 5.84 g of ethylenediaminetetraacetic acid (EDTA) (99 + %, Aldrich), 10.9 g of tris(hydroxymethyl)aminomethane (TRIS) (99.9 + %, Merck) in 100 mL deuterium oxide (D_2O) (99.9 atom %, Cambridge Isotope) and 800 mL MilliQ water. The pH of the DOC buffer was adjusted to pH 9.00 with a 4 M potassium hydroxide solution. After 1 h mixing by vortex the resulted samples were centrifuged and 600 μL of the bottom PL/DOC layer was mixed with 50 μL of an internal standard solution (triisopropyl phosphate (TIP) (96%, Aldrich) in DOC buffer at a concentration of 10 g/L). The samples were measured in standard 5 mm NMR tubes. ^{31}P NMR experiments were performed on a Bruker Avance 400 III HD spectrometer equipped with a CPP BBO 400S1 BB-H&F-d-05 Z ET NMR probe. 1D ^{31}P NMR spectra were measured by at a ^{31}P Larmor frequency of 161.97 MHz and proton decoupling was achieved with the 16 WALTZ sequence. A pulse of 11.45 μs, a relaxation delay (RD) of 11.5 s and 128 scans (NS) were used to record the spectra. The experiments were performed at temperature 27 °C (300 K). Concentrations were determined from the ^{31}P NMR signal ratios of phospholipids and TIP, the internal standard. The detection limit of the ^{31}P NMR method was 40 μmol/100g (0.02w/w%) oil per individual phospholipid and the repeatability was 3–4%.

2.5. Lipid compositional analysis by ^{1}H quantitative NMR

Homogenized gum/oil samples of ~20 mg were mixed with 1 mL of a solvent which included dimethoxybenzene (DMB) (Sigma Chemical Company) as internal standard (1 g/L). The solvent was prepared by mixing chloroform-d ($CDCl_3$) (Cambridge Isotope), methanol-d_4 (MeOH) (Cambridge Isotope), pyridine-d_6 (PYR) (Cambridge Isotope) in the ratio 1:2:0.02 ($CDCl_3$:MeOH:PYR). The samples were measured in standard 5 mm NMR tubes. The 600 MHz ^{1}H NMR experiments were performed on a Bruker Avance 600 III HD spectrometer, equipped with a CP2 TCI 600S3 H−C/N-D05 Z P NMR probe. 1D ^{1}H NMR spectra were measured by applying a pulse of 6 μs, using 8 scans and a recycle delay of 25 s. Concentrations of diglycerides (DGs) and free fatty acids (FFA) were determined via their ^{1}H NMR signal integrals and the one of an internal standard.

2.6. SANS measurements

Small-angle neutron scattering (SANS) measurements were performed at the LARMOR instrument at ISIS neutron and muon source (Didcot, the United Kingdom). The SANS mode of the LARMOR instrument allowed for a total momentum transfer (q) range of 0.004–0.7 $Å^{-1}$. The samples were loaded in 1 mm path length, 1 cm width, quartz Hellma cells, which were placed in a temperature-controlled sample holder. The temperature of the experiments was kept at 20 °C. Data were reduced using the standard routines of Mantid. Data were normalised to sample transmission and corrected for detector efficiencies and the scattering from an empty cell. The scattering of the pure solvents was subtracted accounting for the incoherent contribution to each sample. The output data was absolute scattered intensity, I(q) in cm^{-1}, versus the momentum transfer, q in $Å^{-1}$. The data were analyzed in SasView (www.sasview.org) in order to describe the Bragg peaks. For that the Lamellae and Lamellar_hg_stack_caille models were used where the scale, the spacing of repeated bilayers (d_spacing) and Caille parameters were varied. The fit was used in the range 0.01–0.2 $Å^{-1}$. An average length of a PL tail and an average length of a PL head were estimated as 12.4 Å and 6.8 Å, respectively. The hydrophobic scattering length density (SLD) was estimated $-3.8{\cdot}10^{-6}/Å^2$, hydrophilic SLD was $1.9{\cdot}10^{-6}/Å^2$, and the SLD of the solvent was $6.4{\cdot}10^{-6}/Å^2$.

2.7. SAXS measurements

The small angle X-ray scattering (SAXS) experiments were performed at the European Molecular Biology Laboratory (EMBL, Hamburg) at the beamline P12 (Blanchet et al., 2015). The sample was put in a capillary made of special 'Lindemann' glass (Hilgenberg, Germany) with an outer diameter of 1.5 mm, wall thickness of 0.01 mm and length of 80 mm. Each sample was exposed to the beam for 0.045 s with a wavelength of 0.124 nm. The temperature of the experiments was kept at 22 °C. Data were integrated and reduced using a standard and automated SAXS pipeline routine at P12.

2.8. ^{2}H NMR

The ^{2}H NMR experiments were performed on a Bruker Avance 400 III HD NMR spectrometer equipped with a CPP BBO 400S1 BB-H&F-d-05 Z ET probe. 1D ^{2}H NMR spectra were recorded by at a Larmor frequency of 61.42 MHz, by applying a 90° pulse of 275 μs, using 64 scans and a recycle delay of 1.2 s. The FWHM of the ^{2}H NMR signal was obtained by fitting with a Lorenzian function in MestReNova (Willcott, 2009).

2.9. Time-domain NMR relaxometry

Measurements of spin–spin relaxation times (T_2) were performed on a Maran Ultra NMR spectrometer (Resonance Instruments Ltd., Witney, United Kingdom) at 30.7 MHz ^{1}H resonance frequency (0.72 T magnetic field strength) at a temperature of 2 °C ± 1 °C. To obtain full T_2 relaxation decay curves that cover both the liquid-crystalline and liquid part of the gum/oil system Carr Purcell Meiboom Gill (CPMG) and FID-CPMG pulse sequences were combined. The CPMG decay consisted of 4096 echoes with a dwell time (DW) of 20 μs, 5 points per echo, an echo time of 300 μs and a repetition time of 3 s. Experiments were averaged over 16 scans and repeated five times to define a standard deviation for the fitted T_2 values and populations. The FID-CPMG decay consisted of a FID part measured at DW of 1 μs and with number of points varied between 30 and 70, and a CPMG part with DW of 1 μs, 20 points per echo, TE of 300 μs and with an echo number of 400. There was a constant difference in intensity between the CPMG and FID-CPMG relaxation decays due to the filters used for the sequences. The scaling factor was found as the ratio between CPMG parts of the respective sequences. At a next step, the FID part was adjusted by the scaling ratio. The final relaxation decay was normalised on the highest intensity of the signal. To obtain the T_2 relaxation time distribution in oil/gum systems CPMG relaxation decays were analysed as a continuous distribution of exponents by CONTIN and as a discrete sum of exponents by SplMod (Peters et al., 2016) (Fig. S2, Supplementary material). Quantification of the normalised FID-CPMG relaxation decays was done in Origin (OriginLab, Northampton, MA). By multi exponential fitting of the CPMG part of the relaxation decay a T_2 value and a proton population (p) were obtained for every exponent. The fit of the CPMG decay comprised data points acquired between 0.01 and 1.23 s, which

excluded the FID, and the earliest time points (2–6 ms) since these were sensitive to modulations due to B_1 inhomogeneity. The relaxation decays of the highly lecithin enriched (27.5w/w%) crude oil samples were fitted with the sum of three exponentials, whereas for the lower enriched crude oil samples (12.1w/w% lecithin) and the crude oil required a fit with the sum of four exponentials. The T_2 and p values of the first (shortest T2) CPMG component were attributed to the mobile part of the gum (gum_m), which comprised water and headgroups of PL protons (Fig. 1). The T_2 values of the rigid part of the gum (gum_r), predominantly consisting of packed alkyl chains ofPLs and other amphiphilic lipids, were obtained from the FID part of the relaxation decay by performing a linear fit. The $p(gum_r)$ was obtained from the normalized FID and CPMG data according to equation:

$$p(gum_r) = 1 - p_r(gum_m) - \sum p(oil)$$

where p(oil) corresponded to the protons of oil. The $p_r(gum_m)$ was recalculated from the proton population of the first CPMG component. Small odd–even echo modulations were present in the first points of the CPMG relaxation decay (2–6 ms), these were not corrected for and decays were fitted as is.

2.10. Diffusion-relaxation correlation spectroscopy

A pulsed field gradient stimulated echo NMR pulse sequence (PFG-STE) to measure self-diffusion was combined with a CPMG pulse sequence to measure transversal relaxation. Measurements were performed on a Maran Ultra NMR spectrometer (Resonance Instruments Ltd., Witney, United Kingdom) mentioned above at a temperature of 21 °C ± 1 °C. The PFG-STE sequence was performed with a diffusion encoding time (Δ) of 40 ms, and a PFG duration (δ) of 4 ms. The experiment was repeated 23 times with PFG gradient strengths increasing from 0.12 to 1.11 T/m, using 16 repetitions to improve signal-to-noise, and a repetition time (TR) of 3 s. The CPMG sequence was run as described above. This sequence was analysed using a 2D numerical inverse Laplace transform resulting in a 2D spectrum, showing the correlation between T2 and D (Hürlimann & Venkataramanan, 2002; Song et al., 2002). The 2D datasets were processed in IDL (ITT Visual Information Solution, Boulder, CO USA) and analysed with MATLAB (The MathWorks, Inc., Natick, MA USA) to obtain DRCOSY spectra (Peters et al., 2017). The 2D experiment was performed with Δ values of 40, 80, 120 and 180 ms.

2.11. DOSY

The DOSY experiments were performed on a Bruker Avance 400 III HD NMR spectrometer equipped with a PH MIC 400S1 DIFF/30 probe with maximum gradient 18 T/m. 1D ^{1}H NMR spectra were recorded by applying a 90° pulse of 13.3 μs. The PFG-STE sequence was performed at $\Delta = 40$ ms and $\delta = 4.16$ ms. The experiment was repeated 128 times with PFG gradient strengths increasing from 0.02 to 3.6 T/m, using 32 repetitions, and TR = 2.31 s. The DOSY experiments were acquired at a temperature of 20 °C ± 1 °C. The analysis of the DOSY was performed in Bruker Dynamics Center 2.5.3.

3. Results and discussion

3.1. Impact of degumming on amphiphilic lipid composition

Quantitative compositional profiles of amphiphilic lipids were obtained by ^{1}H and ^{31}P qNMR. They included (weight) concentrations of phospholipids (PLs), lysophospholipids (LPLs), phosphate compounds, diglycerides (DGs) and free fatty acids (FFAs). Fig. 2 shows the compositional profiles of lipids after water (WD) and enzymatic degumming (ED) by phospholipase C (PLC – red), phospholipase A2 (PLA2 – green) and a mixture of phospholipases Purifine 3G (3G – blue). The chart represents data obtained after the degumming processes performed in the presence of approximately 13w/w% D_2O. These profiles were similar for gums obtained with other D_2O concentrations (Fig. S3, Supplementary material). Compositional analyses for H_2O based samples (Fig. S3, Supplementary material) were also in line with those shown in Fig. 2.

As expected, the PL compositional profiles after WD in the native and lecithin-enriched soybean crude oils consisted of phosphatidylcholine (PC), phosphatidylethanolamine (PE), phosphatidylinositol (PI) and phosphatidic acid (PA). The compositional profiles of amphiphilic lipids after ED were in line with known enzymatic conversion of the respective enzymes used (Fig. 1(A)). The PLA2 ED was accompanied by a PL conversion into LPLs and FFAs. After PLC ED treatments most of PC and PE were converted to 1,2-DG and phosphate compounds (Fig. S3, Supplementary material). As expected, the 3G most efficiently converted all types of PLs into LPLs, DGs and FFAs (Fig. 1(A)) (Sein et al., 2019).

3.2. Microscale structure of gums

Fig. 3 shows polarised light microscopy (PLM) images of gums after WD (A) and PLA2 ED (B) vs PLC (C) and 3G (D) ED processes on crude oil. All of them demonstrate the presence of lamellar liquid-crystalline (LC) phases, schematically represented in Fig. 1(B) (further interpretation of the PLM images can be found in Fig. S4, Supplementary material) (Sein et al., 2019). However, as already stipulated in the introduction, the topology of the lamellar phases varies for all studied samples. The WD gum shows a more planar structure on the microscale, whereas the images of the ED gums indicate the presence of spherulites that consist of curved bilayers. These could be formed because the average molecular shape of the polar lipids formed upon PLC and 3G ED treatments become more a truncated-cone like (Sein et al., 2019; van Nieuwenhuyzen & Tomás, 2008). Fig. 3(E, F) shows EM images of gum formed after 3G ED on crude oil. The electron microscopy (EM) images revealed a layered morphology on the submicron scale (Fig. 3(E), (F)). The layer thickness is estimated to be in the order of 100–200 Å. From the PLM and EM images obtained for other degumming treatments we concluded that they all resulted in gums with lamellar LC phases, but all with a different lamellar topology. The PLM and EM images only allow for a qualitative view on submicron structures and could not resolve structural features at the nanometer scale. For further characterisation and quantification of the structural features of gums we have therefore used SANS, SAXS and NMR techniques.

3.3. Impact of degumming on gum mesostructure

SANS and SAXS were used to characterize and quantify the structural differences at mesoscale between gums obtained after WD and ED. Typical SANS scattering curves of gums after WD and ED are shown in Fig. 4(A). D_2O based samples provided a good contrast between amphiphilic lipid and water layers and this allowed for accurate determination of their repeating distances (Fig. 1). The repeating bilayer structures manifested themselves by first and the second order Bragg peaks (Fig. 4(A)). Their positions were reciprocal to spacings d between the bilayers (Nieh, Glinka, Krueger, Prosser, & Katsaras, 2001; Pottage et al., 2014).

The positions of the first and the second order peaks observed for the WD and PLA2 ED gums differed by a factor of two, which indicated planar lamellar LC structures at the *meso* scale. The curvature of the lamellar structures, as shown in the Fig. 3, occurs at a much larger length scale (micron scale) than the repeating distance obtained by SANS. For lamellar LC phases obtained after WD and PLA2 ED conditions, the spacings were in the range from 70 Å to 120 Å for low and high D_2O/PL ratios, respectively. For the samples obtained after the PLC and 3G ED treatments, the Bragg peaks were broad, pointing to the less ordered and heterogeneous structures, and/or highly flexible,

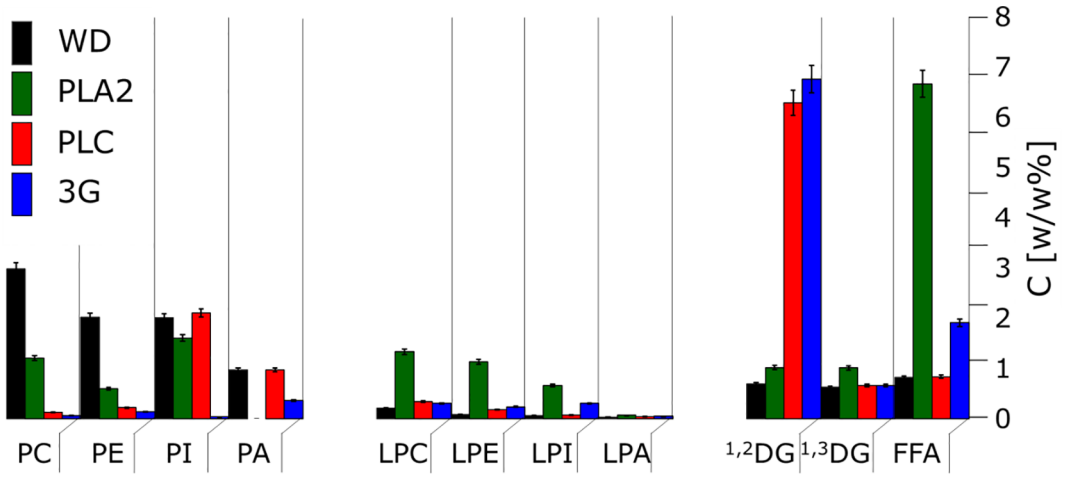

Fig. 2. Phospholipid (PL: PC, PE, PI, PA), lysophospholipid (LPL: LPC, LPE, LPA, LPI), 1,2- and 1,3-diglyceride (1,2- and 1,3-DG) and free fatty acid (FFA) compositions in w/w% after WD (black) and ED PLC (red), PLA2 (green) and 3G (blue). The samples were prepared based on D_2O. The weighed in D_2O concentration was approximately 13w/w%, and PL concentration was between 10 and 11w/w%. Compositional data were obtained by ^{31}P and ^{1}H qNMR with a repeatability of 3–4% (error bars). (For interpretation of the references to colour in this figure legend, the reader is referred to the web version of this article.)

undulating bilayers. The Bragg peaks were shifted to the lower q range, corresponding to spacings in the range of 100–170 Å – depending on the D_2O/PL ratios.

Besides SANS experiments with D_2O based samples we also performed SAXS experiments where we could use samples prepared with H_2O. The spacings deduced from these SAXS experiments were in line with the SANS results and can be found in Fig. S5 (Supplementary material). Given the higher quality of the SANS curves, due to the contrast provided by using D_2O, we continued our analysis using these results. The slopes of the SANS curves at small q-values ($<10^{-2}$ Å) differed significantly between samples and their replicates, indicating strong heterogeneity at the (sub)-micron scale. Hence, we refrained from attempts to characterize the gum structure at this length scale.

In order to establish the impact of ED on gum mesostructure, we assessed by ^{1}H and ^{31}P qNMR differences in amphiphilic lipid composition of the separated gum and oil phases. As expected the separated oil phase contained amounts of PLs and LPLs which were below the reported detection limit of the ^{31}P NMR method of 40 μmol/100 g (0.02w/w%). Hence we assumed that both compound classes almost exclusively ended up in the gum phase. The presence of triglycerides (TG) in the gum phase indicated that part of the oil phase was entrained there. As a consequence, we should also find DGs and FFAs in the gum since these are oil soluble.

We did however find different molar ratios between triglycerides (TGs), DGs and FFAs in the separated oil and gum phases. Since the DG and FFA concentrations should be equal in the separated bulk oil and in the oil entrained in the gum, we can estimate their concentrations in the bilayer phase (Fig. S6, Supplementary material). We found that gums were up to 25% enriched by DGs and FFAs, and hypothesized that these were present as structural component in the bilayer parts.

Fig. 4(B) presents the correlation between spacings d deduced from the well-assigned SANS Bragg peaks and the ratio between water and the amphiphilic lipids present in the WD and ED gums. The amphiphilic lipid compositions were assumed to consist of PLs, LPLs and 25% of DGs and FFAs. Overall, the relations between spacings and water/amphiphilic lipid ratio were different for WD and PLA2 ED vs PLC and 3G ED. In the case of WD and PLA2 ED the ratio between water (D_2O) and amphiphilic components were defined mainly by PLs and LPLs and FFAs (for PLA2) (Fig. 2), since DGs were absent for these treatments. The observed linear dependence was in line with thicker water layers between PL and LPL headgroups with increasing water concentrations (Lei et al., 2003; Rand, 1989). For the PLC and 3G ED treatments also thicker water layers were found, and the ratio between water and amphiphilic components was impacted by the relative high amount of DGs expected to contribute to the bilayers – see above. We note that for the low PL and LPL levels after PLC and 3G ED treatments also the impact of other polar lipids, such as glycolipids, cannot be neglected. The obtained results for PLC and 3G ED indicate that upon hydrolysis of the majority of PLs part of the resulting DGs become incorporated into the lamellar LC phase. Fig. 4(B) shows that this leads to increased spacings compared to the lamellar structures produced by WD and PLA2 ED, which can be attributed to the enhanced hydration capacity of the bilayer (Rand, 1989). The incorporation of DGs and FFAs in the bilayers may also be a main contributor to the highly flexible and possibly undulating nature of the bilayers of the gum phases after 3G or PLC ED. Such undulations may cause further bilayer-bilayer repulsions, and hence to the observed thicker water layers.

3.4. Assignment of populations in time-domain relaxation NMR decays

Time-domain NMR relaxometry experiments were performed in order to quantify mobility and phase composition of the oil-gum systems. The concentration of different phases in the oil-gum systems was quantified via their proton populations and their mobility via the T_2 transverse relaxation times. A multicomponent fit with 4–5 exponentials was performed on the FID and CPMG relaxation decays recorded on native and lecithin-enriched crude soybean oils upon WD and ED in the presence of H_2O. The FID part was described with one fast-relaxation component, where T_2 values were in order of 15–20 μs, with proton populations p in the range of 1–13% of the total proton population (Fig. S2, Supplementary material). This component represented the most rigid part of the gum (gum_r) and was assigned to protons from packed alkyl chains within the bilayers (Fig. 1(B)).

The first components of the CPMG decay had T_2 values in the range of 12–45 ms and populations p between 2 and 35% of the total proton population, these varied with the water concentrations used for WD and ED (Fig. S2, Supplementary material). The T_2 values of this component correlated with reciprocal values of a full width at half maximum (FWHM) of ^{2}H NMR spectral lines of gums prepared with D_2O (Fig. S7). This correlation indicated that this CPMG component for a major part represented protons of water between the bilayers (Fig. 1(B)). Their short T_2 values could be explained by surface relaxation at the bilayer interface with its strongly hydrated headgroups. This finding was corroborated by 2D diffusion-relaxation correlation experiments, where T_2 values of water and oil components were distinguished based on self-diffusion coefficients (Fig. S8, Supplementary material). DOSY

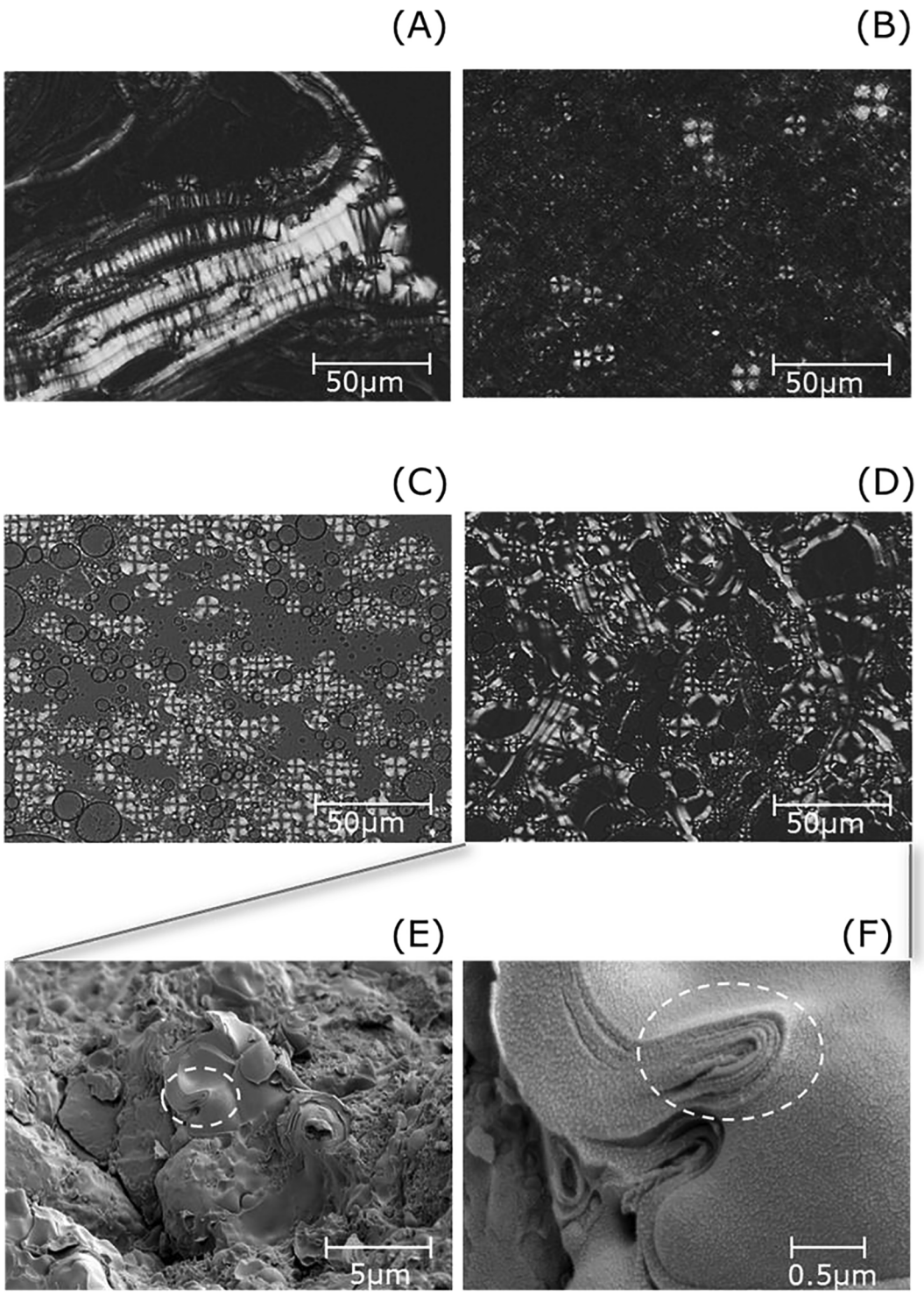

Fig. 3. Polarized light microscopy (PLM) images obtained for gums after water degumming (WD) (A), PLA2 (B), PLC (C) and 3G (D) enzymatic degumming (ED) treatments. Electron microscopy (EM) images (E) and (F) of gums after 3G ED treatment.

experiments in addition, showed that the first CPMG component also included protons from the headgroups of the amphiphilic lipids of the gum. The 2D DOSY plots, where ^{1}H NMR spectra were separated based on self-diffusion coefficients, showed an overlap of water and alkyl chain methylene signals in the range of 4.5–5.5 ppm (Fig. S8, Supplementary material). This indicated that the first T_2 CPMG component comprised both water and mobile head groups of PLs, collectively making up the mobile part of the gum (gum_m).

The other CPMG components were believed to correspond to the neutral oil in the WD and ED samples (Fig. S2, Supplementary material). For the crude oil in native form and enriched with 12.1w/w% lecithin, three components with T_2 values of 53, 110 and 270 ms were needed to describe the remainder of the CPMG decay. For highly lecithin-enriched (27.5w/w%) crude oil samples, only two components (85 and 260 ms) could be resolved for the smaller oil signal. The T_2 values of the neutral oil components (the bulk oil) were stable and did not depend on type of degumming treatments (Fig. S2, Supplementary material).

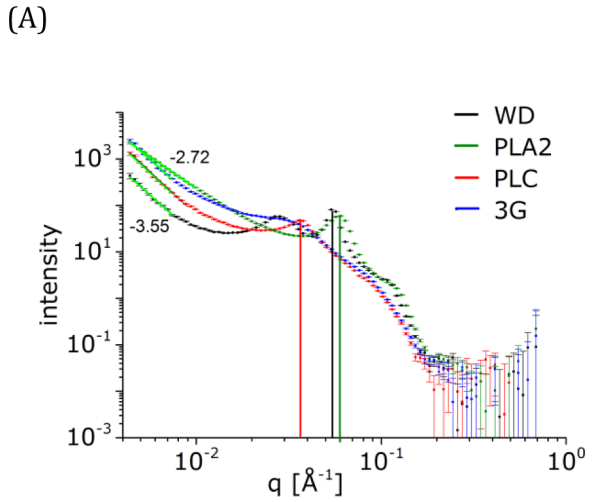

Fig. 4. (A) SANS scattering curves of crude oil with weighed in water and lecithin concentrations of order 13 and 27.5w/w%, respectively, after water degumming (WD – black), phospholipase C (PLC – red), phospholipase A2 (PLA2 – green) and their mixture Purifine 3G (3G – blue) enzymatic degumming (ED) treatments. The vertical lines correspond to the Bragg peaks resulting from repeating bilayers d. (B) Dependencies of the spacings d on ratios between D_2O and amphiphilic compounds including 25% of DGs and FFAs. The PL, LPL, DG and FFA weighted concentrations were obtained by ^{31}P and ^{1}H qNMR compositional analysis. The dashed line is intended to guide the eye. (For interpretation of the references to colour in this figure legend, the reader is referred to the web version of this article.)

The transversal relaxation rates ($1/T_2$) of the gum_m for WD and ED correlated with the reciprocal SANS spacings d (Fig. 5). This was in line with transversal relaxation of water layers between the bilayers of amphiphilic lipids being determined by surface-to-volume ratio. The relaxation rates were grouped in two different dependencies on the bilayer thickness, one for WD and PLA2 ED and one for PLC and 3G ED. This indicated that the mesophases formed by these two groups of degumming treatments differed with respect to surface relaxation of the hydration water at the interface with the headgroups of the amphiphilic bilayers. This result is in line with the different dependencies of the bilayer spacing on water content in the gum for the different treatments (Fig. 4(B)).

3.5. Quantification of gums by time-domain NMR relaxometry

We compared the sum of the $p(gum_r)$ and $p(gum_m)$ proton populations for the full system consisting of oil and gum by TD-NMR

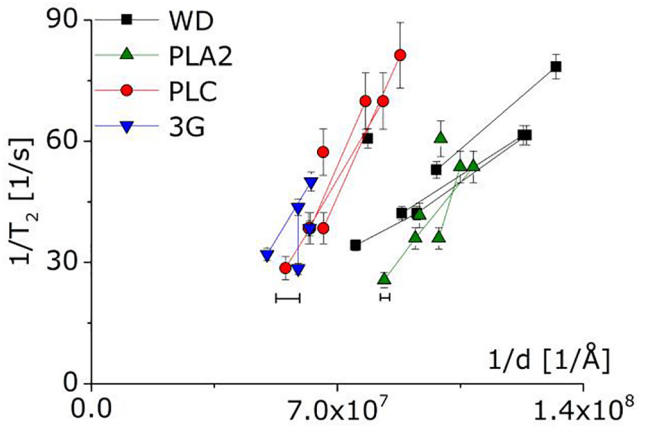

Fig. 5. Correlation between the transverse relaxation rate ($1/T_2$) of the water layers with partly amphiphilic lipid elements and the reciprocal SANS spacings d. The figure presents data obtained after water degumming (WD – black), phospholipase C (PLC – red), phospholipase A2 (PLA2 – green) and Purifine 3G (3G – blue) enzymatic degumming (ED) treatments. (For interpretation of the references to colour in this figure legend, the reader is referred to the web version of this article.)

relaxometry, with the (weight) concentrations of water and amphiphilic lipid components, as obtained by ^{31}P and ^{1}H qNMR (Fig. 6(A)). A well-defined correlation was observed. This confirmed that the gum mesophase consisted of water and PLs, LPLs, DGs and FFAs. We note that the majority of the DGs and the FFAs still partitioned in the bulk oil phase. The correlation also demonstrated that TD-NMR T_2 relaxometry could be used as a method for quantitative assessment of the gum phase in gum/oil dispersions. In order to assess whether TD-NMR relaxometry has a potential to predict the efficiency of degumming treatments, we considered the $p(gum_r)$ population (Fig. 1(B)) as a measure of amphiphilic lipids present in lamellar structures. The rationale was that since $p(gum_r)$ reflected alkyl chains, present in ordered and relatively structured, rigid bilayers (compared to bulk oil), it could be taken as a measure for the amount of amphiphilic lipids that could be separated by gravitational forces. Fig. 6(B) shows $p(gum_r)$ populations of gums after WD and ED treatments on crude oil enriched with 27.5w/w% of PLs at different water concentrations.

The $p(gum_r)$ populations were plotted as a function of the ratio between initial concentrations of H_2O and amphiphilic compounds in gums, before WD and ED treatments. The decrease in $p(gum_r)$ population for WD gums followed the decrease in initial weight fraction of amphiphilic lipids due to the increased water concentration (Fig. 6(B)). This validated that the amphiphilic lipids fully ended up in the bilayers of the gum phase for the WD treatment. For the ED treatment we observed an overall decrease of the $p(gum_r)$ populations. This indicated that less amphiphilic lipids were incorporated in the lamellar LC gum phase which is in line with the enzymatic conversion of amphiphilic lipids. The decreased amount of lamellar LC phase as reflected in p (gum_r) populations followed the order WD, PLA2, PLC and 3G, which was in line with the expected efficiency of enzymatic conversions of the initially present PLs (Figs. 1(A) and 2).

For lower initial levels of PLs the observed effects on $p(gum_r)$ were smaller compared to experimental error, but still we could discern similar trends as shown in Fig. 6(B). Further investigations are necessary to explore whether the separation efficiency of gums from oil after WD and ED can quantitatively be monitored via TD-NMR assessment of p (gum_r) populations.

4. Conclusions

In line with our starting hypothesis both WD and ED resulted in gum phases composed of amphiphilic lipids, which form lamellar liquid-

(A)

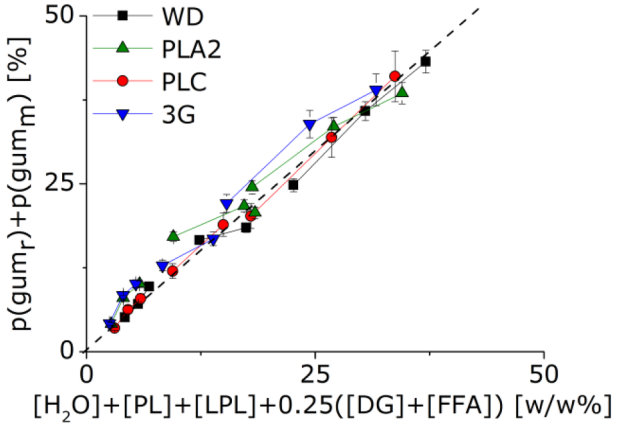

(B)

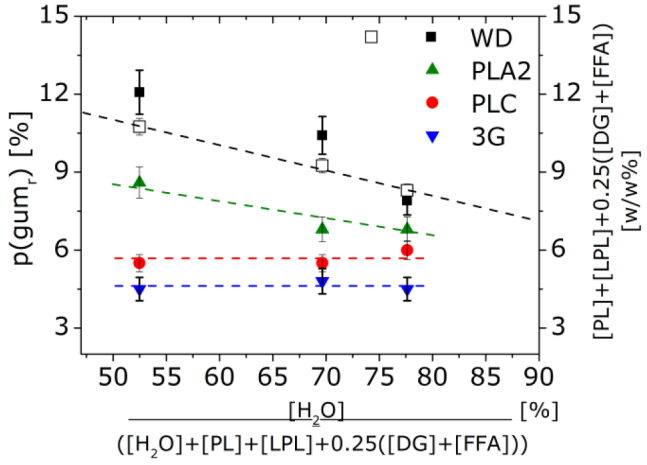

Fig. 6. (A) Correlation between mesophase mass concentrations as determined by time-domain (TD) NMR relaxometry (vertical axis) and compositional analysis by ^{31}P and ^{1}H NMR (horizontal axis). The quantification by TD-NMR relaxometry is based on the amplitudes of proton populations p with T_2 relaxation times of 15–20 μs (gum_r) and 12–45 ms (gum_m). The concentration on the horizontal axis comprises water and amphiphilic lipids (phospholipids (PLs), lysophospholipids (LPLs), diglycerides (DGs), free fatty acids (FFAs)). (B) Dependencies of $p(gum_r)$ populations for WD and ED gums (left axis) on ratio between initial concentrations of H_2O and amphiphilic compounds in gums before enzymatic conversions. The data were obtained for the crude oil enriched with 27.5w/w% PLs. The PL, LPL, DG and FFA weighted concentrations were obtained by ^{31}P and ^{1}H qNMR compositional analysis of the enriched crude oil. The straight line and black empty squares represent the starting concentrations (before degumming) of PL, LPL, DG and FFA compounds (right axis). The figure presents data obtained after water degumming (WD – black), phospholipase C (PLC – red), phospholipase A2 (PLA2 – green) and their mixture Purifine 3G (3G – blue) enzymatic degumming (ED) treatments. The dashed lines are intended to guide the eye. (For interpretation of the references to colour in this figure legend, the reader is referred to the web version of this article.)

crystalline phases. The impact of ED on bilayer curvature could only be confirmed by microscopy. SAXS and SANS showed that gums formed by PLC and 3G ED were more swollen as compared to those formed by WD and PLA2 ED. Compositional analysis of the separated oil and gum phases indicated that this distinct difference between these two types of gums could be attributed to incorporation of DGs and FFAs in bilayers of gums formed by PLC and 3G ED. Time-domain (TD) NMR relaxometry showed that this also introduced more effective surface relaxation for the hydration layers in these gums. Degumming treatments can therefore be differentiated by molecular mobility within the amphiphilic bilayers. Both the total amount of gum as well as the amount of amphiphilic lipids in the gum can be determined by means of TD FID-CPMG relaxation NMR, which opens the opportunity to assess the efficiency of degumming treatments.

Author contributions

TN, AS, HVA and JvD designed the research; TN, TR, WB and AS performed the experiments; TN, AS, WB, HVA and JvD interpreted the results, TN wrote the manuscript, AS, HVA, WB and JvD edited and approved the final manuscript.

Declaration of Competing Interest

The authors declare the following financial interests/personal relationships which may be considered as potential competing interests: TR and AS are employed by a company that produces and markets enzyme products for enzymatic degumming of crude oils.

Acknowledgements

Adam Washington (LARMOR 247 beamline, ISIS neutron and muon source, UK) is acknowledged for his help and technical assistance during SANS experiments. The synchrotron SAXS data was collected at beamline P12 operated by EMBL Hamburg at the PETRA III storage ring (DESY, Hamburg, Germany). We would like to thank Dmitry “Dima” Molodenskiy for the assistance in using the beamline. Myraise van Stijn, Pierre Noirez (DSM, Geleen) acquired electron microscopy micrographs. Remco Muntendam, Tony van den Burg are acknowledged for help and technical assistance during preparation of gum samples after different types of degumming treatments.

Funding

This work is part of the SSCANFOODS (project number 13386) research program, which is financed by The Netherlands Organization for Scientific Research (NWO).

Appendix A. Supplementary data

Supplementary data to this article can be found online at https://doi.org/10.1016/j.foodchem.2019.126017.

References

Blanchet, C. E., Spilotros, A., Schwemmer, F., Graewert, M. A., Kikhney, A., Jeffries, C. M., ... Svergun, D. I. (2015). Versatile sample environments and automation for biological solution X-ray scattering experiments at the P12 beamline (PETRA III, DESY). *Journal of Applied Crystallography, 48*(2), 431–443. https://doi.org/10.1107/s160057671500254x.

Cerminati, S., Paoletti, L., Aguirre, A., Peirú, S., Menzella, H. G., & Castelli, M. E. (2019). Industrial uses of phospholipases: Current state and future applications. *Applied Microbiology and Biotechnology, 103*(6), 2571–2582. https://doi.org/10.1007/s00253-019-09658-6.

Dayton, C. L. G., & Galhardo, F. (2014). Enzymatic degumming. *Green Vegetable Oil Processing, 107–145*. https://doi.org/10.1016/B978-0-9888565-3-0.50009-1.

Dijkstra, A. J. (n.d.). Edible Oil Processing: Introduction to Degumming. Retrieved from http://lipidlibrary.aocs.org/OilsFats/content.cfm?ItemNumber=40325.

Dijkstra, A. J. (2011). Enzymatic degumming. *Lipid Technology, 23*(2), 36–38. https://doi.org/10.1002/lite.201100085.

Hürlimann, M. D., & Venkataramanan, L. (2002). Quantitative measurement of two-dimensional distribution functions of diffusion and relaxation in grossly inhomogeneous fields. *Journal of Magnetic Resonance, 157*(1), 31–42. https://doi.org/

10.1006/jmre.2002.2567.
Jiang, X., Chang, M., Wang, X., Jin, Q., & Wang, X. (2014). A comparative study of phospholipase A1 and phospholipase C on soybean oil degumming. *JAOCS, Journal of the American Oil Chemists' Society, 91*(12), 2125–2134. https://doi.org/10.1007/s11746-014-2555-6.
Kučerka, N., Pencer, J., Sachs, J. N., Nagle, J. F., & Katsaras, J. (2007). Curvature effect on the structure of phospholipid bilayers. *Langmuir, 23*(3), 1292–1299. https://doi.org/10.1021/la062455t.
Lei, L., Ma, Y., Kodali, D. R., Liang, J., & Ted Davis, H. (2003). Ternary phase diagram of soybean phosphatidylcholine-water-soybean oil and its application to the water degumming process. *JAOCS, Journal of the American Oil Chemists' Society, 80*(4), 383–388. https://doi.org/10.1007/s11746-003-0708-y.
Nagle, J. F., & Tristram-Nagle, S. (2000). Structure of lipid bilayers. *Biochimica et Biophysica Acta – Reviews on Biomembranes, 1469*(3), 159–195. https://doi.org/10.1016/S0304-4157(00)00016-2.
Nieh, M.-P., Glinka, C. J., Krueger, S., Prosser, R. S., & Katsaras, J. (2001). SANS study of the structural phases of magnetically alignable lanthanide-doped phospholipid mixtures. *Langmuir, 17*(9), 2629–2638. https://doi.org/10.1021/la001567w.
Peters, J. P. C. M., Vergeldt, F. J., As, H. Van, Luyten, H., Boom, R. M., Jan, A., & Goot, V. Der (2016). Food hydrocolloids time domain nuclear magnetic resonance as a method to determine and characterize the water-binding capacity of whey protein microparticles. *Food Hydrocolloids, 54*, 170–178. https://doi.org/10.1016/j.foodhyd.2015.09.031.
Peters, J. P. C. M., Vergeldt, F. J., As, H. Van, Luyten, H., Boom, R. M., Jan, A., & Goot, V. Der (2017). Food hydrocolloids unravelling of the water-binding capacity of cold-gelated whey protein microparticles. *Food Hydrocolloids, 63*, 533–544. https://doi.org/10.1016/j.foodhyd.2016.09.038.
Pottage, M. J., Kusuma, T., Grillo, I., Garvey, C. J., Stickland, A. D., & Tabor, R. F. (2014). SI_Fluorinated lamellar phases: structural characterisation and use as templates for highly ordered silica materials. *Soft Matter, 2014*, 1–2. https://doi.org/10.1039/c4sm00666f.
Rand, R. (1989). (CUL-ID:1654990) Hydration forces between phospholipid bilayers. *Biochimica et Biophysica Acta (BBA) – Reviews on Biomembranes, 988*(3), 351–376. https://doi.org/10.1016/0304-4157(89)90010-5.
Rijn, J. H. J., Lankhorst, P. P., Groen, P. B. M., Muntendam, R., & Souza, A. C. (2019). Robust and reliable quantification of phospholipids in edible oils using 31 P NMR spectroscopy. *Journal of the American Oil Chemists' Society*. https://doi.org/10.1002/aocs.12296 JAOCS.12296.
Sagalowicz, L., Moccand, C., Davidek, T., Ghanbari, R., Martiel, I., Negrini, R., ... Michel, M. (2016). Lipid self-assembled structures for reactivity control in food. *Philosophical Transactions A, 374*, 20150136. https://doi.org/10.1098/rsta.2015.0136.
Sein, A., Hitchman, T., & Dayton, C. L. G. (2019). Enzymes in vegetable oil degumming processes. In A. Vogel, & O. May (Eds.). *Industrial Enzyme Applications* (pp. 323–350). Wiley-VCH.
Sen Gupta, A. K. (1986). Neuere Entwicklungen auf dem Gebiet der Raffination der Speiseöle. *Fette Seifen Anstrichm, 88*, 79–86. https://doi.org/10.1002/lipi.19860880302.
Song, Y. Q., Venkataramanan, L., Hürlimann, M. D., Flaum, M., Frulla, P., & Straley, C. (2002). T1–T2 correlation spectra obtained using a fast two-dimensional Laplace inversion. *Journal of Magnetic Resonance, 154*(2), 261–268. https://doi.org/10.1006/jmre.2001.2474.
Van Duynhoven, J., van Velzen, E., & Jacobs, D. M. (2013). *Quantification of complex mixtures by NMR. Annual Reports on NMR Spectroscopy, Vol. 80*1st ed: Elsevier Ltd Doi: 10.1016/B978-0-12-408097-3.00003-2.
van Nieuwenhuyzen, W., & Tomás, M. (2008). Update on vegetable lecithin and phospholipid technologies. *European Journal of Lipid Science and Technology, Vol 110*. https://doi.org/10.1002/ejlt.200800041.
Willcott, M. R. (2009). MestRe Nova. The Journal of the American Chemical Society, 906709–906709. https://doi.org/10.1021/ja906709t.
Xie, M., & Dunford, N. T. (2017). Lipid composition and emulsifying properties of canola lecithin from enzymatic degumming. *Food Chemistry, 218*, 159–164. https://doi.org/10.1016/j.foodchem.2016.09.074.
Ye, Z., Qiao, X., Luo, Z., Hu, C., Liu, L., & He, D. (2016). Optimización y comparación del desgomado con agua y el desgomado con fosfolipasa C de aceite de colza. *CYTA – Journal of Food, 14*(4), 604–612. https://doi.org/10.1080/19476337.2016.1182218.